Engineering Structures 283 (2023) 115868

Contents lists available at ScienceDirect

Engineering Structures

journal homepage: www.elsevier.com/locate/engstruct

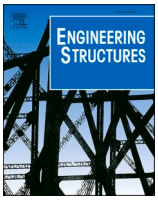

Seismic mitigation of a benchmark twenty-story steel structure based on intermodal targeted energy transfer (IMTET)

Majdi Gzal [a,*], Juan E. Carrion [b], Mohammad A. AL-Shudeifat [c], Billie F. Spencer Jr [d], Joel P. Conte [e], Alexander F. Vakakis [f], Lawrence A. Bergman [g], Oleg V. Gendelman [a]

[a] Department of Mechanical Engineering, Technion – Israel Institute of Technology, Haifa, Israel
[b] Department of Civil Engineering, University of Cuenca, Cuenca, Ecuador
[c] Department of Aerospace Engineering, Khalifa University, Abu Dhabi, United Arab Emirates
[d] Department of Civil and Environmental Engineering, University of Illinois, Urbana, USA
[e] Department of Structural Engineering, University of California, San Diego, USA
[f] Department of Mechanical Science and Engineering, University of Illinois, Urbana, USA
[g] Department of Aerospace Engineering, University of Illinois, Urbana, USA

ARTICLE INFO

Keywords:
Seismic excitation
Intermodal targeted energy transfer (IMTET)
Vibro-impacts
Hertzian contacts
Passive mitigation

ABSTRACT

This study investigates a new intermodal targeted energy transfer (IMTET) concept for rapid, effective, and purely passive seismic mitigation of a benchmark large-scale model of a twenty-story steel structure. IMTET is based on extremely rapid nonlinear scattering of seismic input energy from low to high frequency modes of a building. This effect is achieved by introducing strategically placed, local strong vibro-impact nonlinearities that are generated by contacts of the building floors with a relatively light, yet stiff, auxiliary core structure. Accordingly, the performance of IMTET is studied here, with the benchmark structure realized through a set of previously established performance criteria. The seismic loads are simulated based on records from three historical earthquakes, namely the 1995 Kobe, 1994 Northridge, and 1940 El Centro. To assess the robustness of the proposed passive nonlinear mitigation mechanism, the clearance distributions as well as the core structure parameters, are optimized for a specific seismic excitation (Kobe). Subsequently, the optimized design is tested against the two other historical earthquake records to demonstrate the effectiveness of the IMTET for these cases as well. The numerical results show that the vibro-impacts rapidly, robustly, and almost irreversibly redistribute the seismic input energy from low to high frequency structural modes, thus realizing a highly effective passive earthquake protective system. In addition, when optimized, this new concept can be realized fully passively, without the need to add any mass to the building, and at the cost of only moderate increases in the resulting floor accelerations and local stresses. In addition, the nonlinear vibro-impacts between the floors and the core structure reduce the seismic input energy to the building compared to the no core case, adding an additional benefit to the seismic mitigation approach. Therefore, the IMTET methodology for seismic mitigation has the potential to significantly enhance the seismic performance of building structures.

1. Introduction

Earthquakes can cause massive loss of life and property in highly populated areas, as exemplified by the Northridge earthquake (1994), the Kobe earthquake (1995) and the Sichuan earthquake (2008) in the US, Japan, and China, respectively. Conventional design for extreme loading scenarios is predicated upon the notion that structures passively resist environmental forces through a combination of strength, ductility, and energy absorption. As such, a significant portion of the seismic input energy is absorbed by the structure itself through local damage, e.g., in plastic hinge regions of beams, bracing elements, shear walls, and so forth. It is paradoxical then that the deleterious effects of the earthquake are counteracted by allowing structural damage.

An alternative approach to mitigate the effects of these extreme loads is to absorb or reflect a portion of the input energy, not by the structure itself, but by some type of protective system. This approach can be explained through the following energy conservation relation [1]:

* Corresponding author.
E-mail address: majdi.gzal@technion.ac.il (M. Gzal).

https://doi.org/10.1016/j.engstruct.2023.115868
Received 23 August 2022; Received in revised form 18 January 2023; Accepted 17 February 2023
Available online 2 March 2023

$$E = E_k + E_h + E_s + E_d \quad (1)$$

where E is the total input energy, E_k the kinetic energy, E_h the non-recoverable energy dissipated by the structure through material hysteresis or other intrinsic dissipative effects, E_s the recoverable elastic strain energy, and E_d the energy dissipated by the protective system. Consequently, many innovative structural protection concepts have been proposed, developed, and even implemented, being classified as passive, semi-active, and fully active.

Briefly, passive protective systems reduce the energy dissipation demand on the structure by reflecting or absorbing and dissipating a portion of the input energy. However, these systems typically are not robust to large variability in loading characteristics. Active protective systems, on the other hand, can readily adapt to large load variability to produce near-optimal performance over a broad range of metrics [2]; but such optimal performance happens at the expense of cost, reliability, durability, maintainability, and power requirements associated with arrays of sensors and actuators that algorithmically adjust in real-time the dynamic properties of the system. Semi-active protective systems provide a kind of compromise, because they do not apply energy to the structure but can intelligently store and dissipate energy from it, using actuators requiring only a modest amount of power to algorithmically adjust in real-time their material and/or mechanical properties. However, as with fully active systems, reliability and maintainability remain an issue, e.g., due to the long-duration intervals between short and intense periods of activity. Despite intensive research over the past several decades, active and semi-active strategies have been slow to gain wide acceptance, with fully passive protective systems most often being preferred.

One of the more popular passive protective strategies, particularly for low- and medium-rise buildings, is base isolation, alternately denoted by seismic isolation. Here, the isolation system is typically placed between the structure and its foundation to introduce flexibility and energy absorption capability (see Fig. 1a). The isolation system acts to partially reflect and absorb the seismic input energy before it can be transmitted to the structure. The most important design characteristic of the isolation system is its flexibility, which introduces a new low frequency "rigid-body" mode, well below the structural modes; such a low frequency mode promotes vibration isolation, sufficient stiffness under service loads and ambient vibrations, and significant energy dissipation capacity [3]. Reported examples in the US include the Salt Lake City Building [4,5]. Typical seismic isolation devices are highly damped elastomeric bearings, lead-rubber bearings, and sliding friction pendulum bearings [6]. External devices based on rotary friction [7], and variable negative stiffness [8] were recently proposed.

Another class of passive protective systems employs supplemental damping devices to increase the energy dissipation capacity of the structure (Fig. 1b). Their basic function is to absorb and dissipate a significant portion of the seismic input energy, thus reducing the energy dissipation demand by the structure itself. This may be achieved by either converting kinetic energy to heat or by transferring energy among the vibration modes. The first method includes devices that operate on principles such as frictional sliding, yielding or phase transformation in metals, and deformation of viscoelastic solids or fluids. Examples include yielding metal dampers, friction dampers, viscoelastic dampers, viscous fluid dampers, and viscously damped walls [9,10]. The second method includes dynamic vibration absorbers, e.g., tuned mass dampers (TMDs – Fig. 1c) [11–16] and tuned liquid dampers [17–20]. Implementations include the system of viscoelastic dampers in the original World Trade Center to reduce wind-induced vibrations [21], and the TMDs installed in the Citicorp Center, both in New York City, the John Hancock Tower in Boston, and the main towers of the Akashi-Kaikyo Bridge near Kobe, Japan [2], to reduce wind-induced vibrations (and also the seismic response) of the bridge. A relatively new approach to limiting lateral forces in earthquake-resistant buildings is the Inertial Force-Limiting Floor Anchorage System (IFAS), described in [22,23]. This is accomplished by introducing compliant damped connections between the flexible gravity load-bearing super-structure and the stiff floor slabs of the earthquake-resistant structure, which, when optimally designed, reduce the inter-story drifts and floor accelerations.

The majority of these passive protective systems was, and continues to be, designed typically based on the theory of linear dynamics, well known to practitioners, despite the obvious nonlinearities, such as those in the dissipative elements due to material behaviour, e.g., hysteresis or friction, which get lumped into an equivalent linear viscous contribution. This design strategy is most effective at (or near) resonances of the structure when it is excited for reasonably long times by narrowband persistent excitations (produced for example by rotating machinery). However, loads produced by shock, blast, and earthquakes are impulsive in nature and, thus, broadband and transient, leaving insufficient time for the damping forces to build up to a level that provides effective mitigation. The alternative, then, excluding the active and semi-active design approaches that, as already mentioned, are not efficient when subjected to rare, extreme loading events, is to extend the passive solution design space *to include intentional strong stiffness nonlinearity in the design of the protective systems*.

The efficacy and wide applicability of a class of relatively lightweight, essentially nonlinear (i.e., non-linearizable at the origin of their stiffness characteristic) absorbers, called nonlinear energy sinks (NES), has been demonstrated in a variety of linear and nonlinear structures, to achieve fully passive mitigation which rivals the performance of active and semi-active protective systems, through targeted energy transfer (TET) [24].

The mechanism of TET was first studied by investigating a strongly nonlinear dissipative oscillator weakly coupled to an impulsively excited linear one. It was shown that, due to nonlinear resonance, the impulsive energy input is irreversibly transferred from the linear to the nonlinear oscillator – acting as the NES, by means of a nonlinear beating phenomenon [25–27]. The main conclusion was that for TET to occur in a system, it must possess strong stiffness nonlinearity which provides the

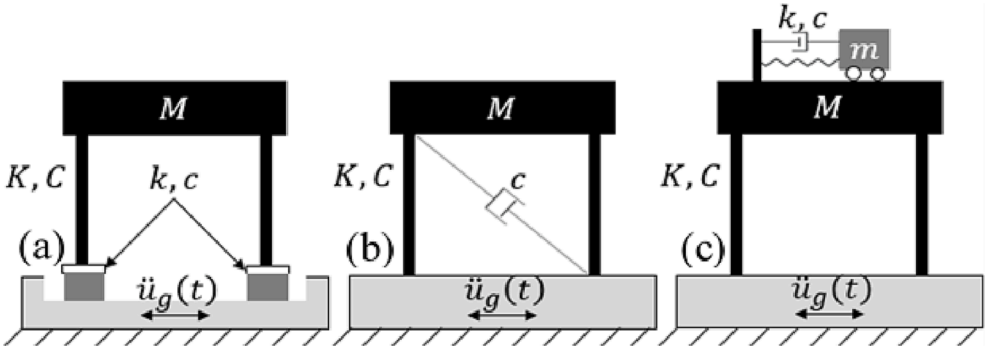

Fig. 1. Passive mitigation systems: (a) base isolation, (b) supplemental damping, and (c) tuned mass damper.

necessary condition for nonlinear resonance, and a dissipation source. Later studies demonstrated that TET can be achieved even when the mass of the NES is significantly smaller than that of the linear oscillator [28–30]. This observation was of particular importance due to its practicality, because it revealed that with the addition of a lightweight NES, one gains the ability to significantly alter the system dynamics and induce intense nonlinear TET [30]. Extending this concept to multi-mode linear structures, the implementation of TET by attaching local NESs to a structure to realize irreversible energy absorption by the NESs, is a fundamental mechanism for realizing TET. This is now a well-accepted passive response mitigation strategy with many documented applications and experimental realizations on multiple platforms across scales [24,31–34]. Recently, the prospective research venues concerning TET in dynamical and acoustical systems were briefly outlined and discussed by Vakakis et al. [35].

However, the traditional approach for achieving TET by means of local NESs, based on a nonlinear resonance mechanism which is realized through slow modulations of the modal amplitudes, occurs on a relatively slow time scale. Therefore, the NES is unlikely to be effective for applications involving extreme loads, e.g., blast or seismic excitations, which require an extremely rapid reaction time for effective energy mitigation, especially in the initial stage of the response when the energy of the system is at its highest level and the potential of structural damage is greatest.

Recent work by the authors, however, has shown that nonlinear resonance is not the only fundamental mechanism for achieving TET, because it can also be realized through a non-resonant mechanism involving non-smooth effects such as vibro-impacts [36]. This effect has been employed to explore computationally the concept of intermodal targeted energy transfer (IMTET) to mitigate the effect of blast loading on a nine-story steel structure [37]. In that study, IMTET was achieved by inducing extremely rapid energy transfers from the low-frequency structural modes directly excited by the blast to higher-frequency structural modes. These transfers were induced by strong inelastic Hertzian vibro-impacts between the nine-story (primary) structure and a secondary, very stiff internal core structure; the optimized clearance distribution resulted in rapid and nearly irreversible scattering of the input blast energy across the entire modal spectrum of the primary structure [37]. In addition, the IMTET was experimentally demonstrated in an impulse-excited cantilever beam system with vibro-impacts [38].

This paper presents an approach and implementation of the IMTET strategy for passive seismic protection of mid- and high-rise buildings subjected to strong earthquakes, which are illustrated for a twenty-story benchmark building. To this end, the work is structured as follows. Section 2 contains the description of the benchmark building, the implementation of the IMTET concept and the governing equations of motion. Then, the computational study and IMTET optimization are detailed in Section 3. Next, the simulation results are presented and discussed in Section 4. Finally, concluding remarks and the envisioned potential applications are discussed in Section 5.

2. Structural model

In this section, a brief review of the benchmark structure is given. The reader is referred to Spencer et al. [39] for further details. Next, a reduced order model is adopted followed by the implementation strategy of IMTET seismic mitigation, and then a mathematical model is formulated. Finally, the considered historical earthquake records, are presented.

2.1. Benchmark structure description

The primary structure considered here is the benchmark 20-story steel building designed by Brandow & Johnston Associates for the SAC Phase II Steel Project [39]. This building is 30.48 [m] by 36.58 [m] in plan, and 80.77 [m] high, and represents a typical mid- to high-rise building designed for the Los Angeles region, meeting seismic code requirements. The building's lateral load-resisting system is comprised of steel perimeter moment-resisting frames (MRFs). For the detailed layout of the building, the reader is referred to Fig. 1 in [39]. Typical floor-to-floor heights are 3.96[m]. The floor-to-floor height for the first floor is 5.49[m]. The floors are composite construction (i.e., concrete and steel). In accordance with common practice, the floor system, which provides diaphragm action, is assumed to be rigid in the horizontal plane. The floor system is comprised of steel wide-flange beams acting compositely with the floor slab.

The seismic mass is $5.32 \times 10^5[kg]$ for the first level, $5.65 \times 10^5[kg]$ for the second level, $5.51 \times 10^5[kg]$ for the third to the 20^{th} levels, and $5.83 \times 10^5[kg]$ for the roof. The seismic mass of the entire structure is $1.16 \times 10^7[kg]$. A finite element (FE) model was developed [39] by employing plane-frame elements. The evaluation model focused on one of the two moment-resisting frames of the 20-story structure, which supports one half of the seismic mass of the entire structure, i.e., $5.80 \times 10^6[kg]$. Then, the mass of the first level was excluded from the model, which, in turn, leads to a final seismic mass of $5.54 \times 10^6[kg]$. Guyan reduction was used to reduce the number of degrees-of-freedom (DOFs) to a manageable size, while still maintaining the important dynamics of the full model, as described in the next section. Using the resulting reduced mass and stiffness matrices, the damping matrix was determined based on the assumption of linear viscous modal damping [40] with a damping ratio of 3% assigned to each mode of the developed reduced-order model.

2.2. Reduced-order model (ROM)

A reduced-order model (ROM) with 106 DOFs of the twenty-story building was developed in [39]. This model is assembled from both horizontal and vertical DOFs. As the vertical dynamic DOFs are unlikely to significantly contribute to the response, they are not required for the benchmark model and can be removed. Eliminating the vertical DOFs results in a ROM with only 62 DOFs, that maintains the important dynamics of the original model. Because each floor slab is assumed to be rigid in its horizontal plane, the horizontal DOFs associated with each floor are identical. This assumption is enforced by writing constraint equations relating the dependent horizontal DOFs on each floor slab to a single active horizontal DOF and using a Ritz transformation [41]. First, the structural responses are partitioned in terms of active and dependent (slave) DOFs, denoted by U_a and U_d, respectively, as $U_{62\times1} = [[U_a]_{1x20}, [U_d]_{1x42}]^T$. Next, the constraint equations are written in the form:

$$R_{da}U_a + R_{dd}U_d = 0 \tag{2}$$

Then, the mass and stiffness matrices are similarly partitioned in terms of active and dependent DOFs:

$$\bar{M}_{62x62} = \begin{bmatrix} \bar{M}^{aa}_{20x20} & \bar{M}^{ad}_{20x42} \\ \bar{M}^{da}_{42x20} & \bar{M}^{dd}_{42x42} \end{bmatrix}, \quad \bar{\mathrm{K}}_{62x62} = \begin{bmatrix} \bar{K}^{aa}_{20x20} & \bar{K}^{ad}_{20x42} \\ \bar{K}^{da}_{42x20} & \bar{K}^{dd}_{42x42} \end{bmatrix} \tag{3}$$

Removing the dependent DOFs yields the following (20 × 20) mass and stiffness matrices:

$$M_{20x20} = T_R^T \bar{M}_{62x62} T_R, \quad K_{20x20} = T_R^T \bar{K}_{62x62} T_R \tag{4}$$

Here, the transformation matrix T_R is given by (where I denotes the unit matrix):

$$T_R = \begin{bmatrix} I_{20x20} \\ T_{da,42x20} \end{bmatrix}_{62x20} = \begin{bmatrix} I_{20x20} \\ \left[-R_{dd}^{-1} R_{da} \right]_{42x20} \end{bmatrix}_{62x20} \tag{5}$$

The mass and stiffness matrices for the reduced order model of the 20-story primary structure are listed in the Appendix below. The damping matrix C_{20x20} is defined based on the reduced system and the assumption of modal damping [40]:

$$C_{20x20} = M_{20x20}\Phi \begin{bmatrix} 2\zeta_1\omega_1 & 0\cdots 0 & 0 \\ \vdots & \ddots & \vdots \\ 0 & 0\cdots 0 & 2\zeta_{20}\omega_{20} \end{bmatrix} \Phi^{-1} \quad (6)$$

where Φ is the matrix of mode shapes (i.e., the eigenvectors of $M_{20x20}^{-1}K_{20x20}$), and ω_i and ζ_i denote the natural frequency and damping ratio, respectively, of the ith mode.

The accuracy of the developed ROM is demonstrated through a comparison of the natural frequencies obtained for the three ROMs of different orders, as shown in Fig. 2(a). In addition, comparisons between the original model with 106 DOFs and the ROM with 20 DOFs in terms of the peak floor relative displacement and peak floor absolute acceleration of each floor as a result of applying the Kobe (1995) earthquake are illustrated in Figs. 2(b) and (c), respectively. It is seen that the ROM with 20 DOFs captures the dynamics of the original model with very good accuracy. Thus, in the sequel, the ROM with 20 DOFs will be considered for investigating the IMTET concept, whereas the final verification will be performed using the original 106 DOFs model.

2.3. Implementation of IMTET seismic mitigation

To implement seismic mitigation using the IMTET concept [37], an additional internal core structure is introduced, with intentional and distributed clearances with respect to the floors of the primary building (Fig. 3), thus inducing vibro-impact (non-smooth) nonlinearities in the structural dynamics, as the structure and core respond to seismic excitations. The clearance gaps will result in a limited number of strong impacts between the floors of the primary building and the core structure. Provided that the seismic input is sufficiently strong, these vibro-impact events will cause rapid "scattering" of the seismic input energy from the lower structural modes of the building (especially the fundamental one) to the higher frequency modes. The anticipated benefits to seismic mitigation are three-fold: (i) as the energy gets transferred from low to high frequencies, the overall envelopes of the structural responses rapidly decreases (because an increase in frequency results in a decrease of vibration amplitudes – and this is achieved even without accounting for energy dissipation due to inherent damping); (ii) the higher structural modes more efficiently dissipate the seismic input energy compared to the lower modes, so the portion of the seismic energy transferred to higher frequencies is dissipated faster and more effectively; and (iii) a significant portion of the seismic energy is rapidly dissipated by few strong inelastic impacts that occur during the highly energetic, initial phase of the structural response. Combined, these effects result in extremely rapid, highly effective, very robust and completely passive seismic mitigation, starting as early as the initial cycle of the structural response. However, special attention must be paid to the resulting acceleration levels resulting from the high momentum floor-to-core impacts in the building, which should be kept within safe design levels (especially for the non-structural components and systems attached to the building structure).

The interactions between the floors of the primary building and the internal core structure are modeled as dissipative Hertzian contacts. Fig. 3a illustrates a phenomenological model of the primary building with the internal core structure subjected to a unidirectional horizontal seismic excitation (i.e., ground motion). It is assumed that both, the building and the core, vibrate only translationally along the loading direction. The displacements of the *jth* floor of the building and core structure with respect to the ground, are denoted by u_j and v_j, respectively, $j = 1, 2, \cdots, 20$. The strong non-smooth nonlinearities required for IMTET are realized by introducing clearance distributions $\Delta_j, j = 1, 2, \cdots, 20$, between the *jth* floors of the building and the core structure, with no other points of contact. Inelastic Hertzian contact forces are assumed, with the nonlinear viscous-elastic dissipative forces modeled after Hunt and Crossley [42]. Based on the required core slenderness, the corresponding mass and stiffness matrices of the core structure were determined using the Euler-Bernoulli beam-column model. It was found that a core with a rectangular cross-section and variable thickness, and therefore varying stiffness and mass properties along the height, is an appropriate design for efficient IMTET with a reasonable core structure mass (Fig. 3b).

The shapes of the first 10 vibrational modes of the primary building (without the core) are schematically shown in Fig. 4. These mode shapes of the primary building are useful later to analyze the structure response to seismic excitation through projection of the nonlinear equations of motion on the mode shapes of the primary building. The frequencies of the leading modes of the primary building, the core structure, and the zero-gap integrated building-core system are listed in Table 1. This last (linear) system is derived when all clearances between floors and the core are eliminated, and, as a result, the core is integrated within the primary building, i.e., resembling a typical combined moment frame with core structure (dual wall-frame structure), for comparison purposes.

2.4. Equations of motion

Denoting by $\boldsymbol{M}$, $\boldsymbol{K}$, $\boldsymbol{C}$, and $\boldsymbol{M_{cs}}$, $\boldsymbol{K_{cs}}$ and $\boldsymbol{C_{cs}}$, the (20 × 20) mass, stiffness and damping matrices of the primary building and the core structure, respectively, the equations of motion are given by,

$$\begin{aligned} \boldsymbol{M}\ddot{\boldsymbol{u}} + \boldsymbol{C}\dot{\boldsymbol{u}} + \boldsymbol{K}\boldsymbol{u} - \boldsymbol{f}^{NL}(\dot{\boldsymbol{u}}, \boldsymbol{u}, \dot{\boldsymbol{v}}, \boldsymbol{v}, \Delta) &= -\boldsymbol{M}\boldsymbol{\Gamma}\ddot{u}_g \\ \boldsymbol{M_{cs}}\ddot{\boldsymbol{v}} + \boldsymbol{C_{cs}}\dot{\boldsymbol{v}} + \boldsymbol{K_{cs}}\boldsymbol{v} + \boldsymbol{f}^{NL}(\dot{\boldsymbol{u}}, \boldsymbol{u}, \dot{\boldsymbol{v}}, \boldsymbol{v}, \Delta) &= -\boldsymbol{M_{cs}}\boldsymbol{\Gamma}\ddot{u}_g \end{aligned} \quad (7)$$

where $\ddot{u}_g$ is the ground acceleration, $\boldsymbol{u}$ and $\boldsymbol{v}$ the relative displacement vectors of the building floors and core contact points, respectively, $\boldsymbol{\Gamma}$ the influence vector of the base motion, and $\boldsymbol{\Delta}$ the vector of clearance gaps. Uniaxial seismic excitation is considered along the short (i.e., weak) direction of the primary building (see Fig. 1 in [39]). The vector

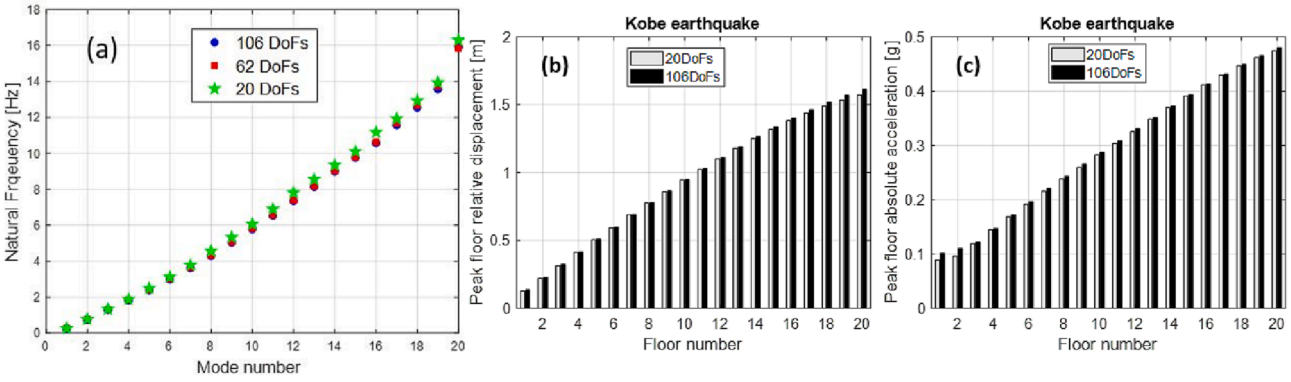

Fig. 2. Comparison between the original model with 106 DOFs and the ROM with 20 DOFs as a result of applying the Kobe (1995) earthquake: (a) natural frequencies [Hz], (b) peak floor relative displacement [m], (c) and peak floor absolute acceleration [g].

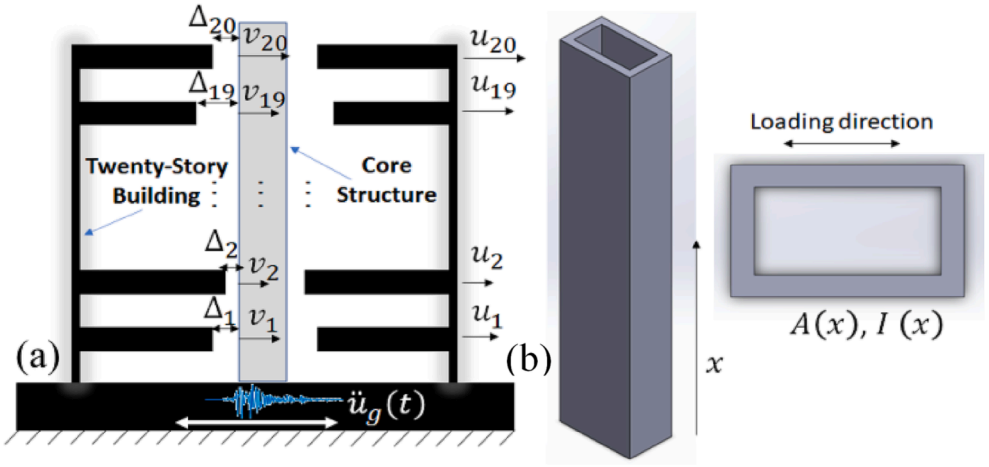

Fig. 3. Seismically excited 20-story primary building with internal core structure: (a) integrated system of building-core, and (b) core structure.

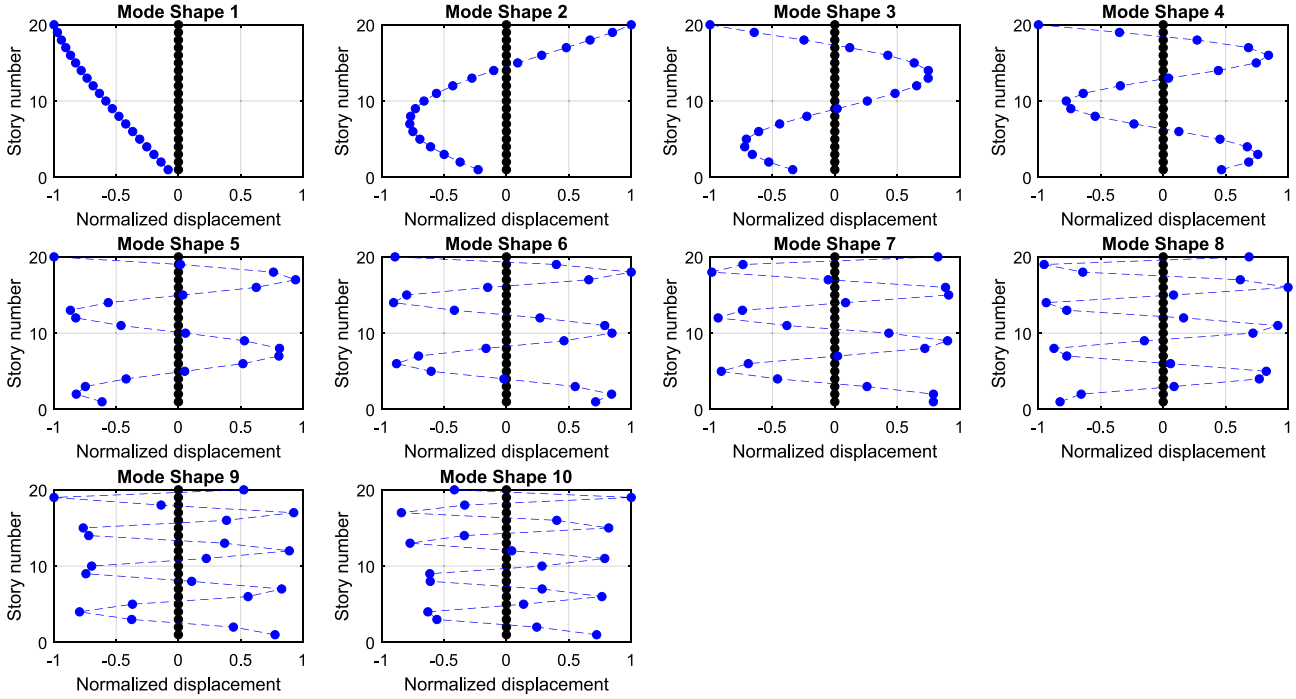

Fig. 4. The first 10 vibrational mode shapes of the primary building.

Table 1
Leading natural frequencies [Hz] of the primary building, core structure, and zero-gap integrated building-core system.

Mode No.	1	2	3	4	5	6	7	8	9	10
Primary building	0.26	0.75	1.30	1.82	2.40	3.00	3.62	4.31	5.04	5.80
Core structure	2.29	13.22	36.19	70.49	116.25	173.48	242.24	322.65	414.91	519.39
zero-gap building-core system	0.75	4.29	11.82	23.08	38.12	56.95	79.55	105.94	136.07	169.91

$\boldsymbol{f}^{NL}(\dot{\boldsymbol{u}},\boldsymbol{u},\dot{\boldsymbol{v}},\boldsymbol{v},\boldsymbol{\Delta})$ contains the inelastic Hertzian contact interactions, and its *jth* element is given by,

$$f_j^{NL}(\dot{\boldsymbol{u}},\boldsymbol{u},\dot{\boldsymbol{v}},\boldsymbol{v},\Delta) = k_c\left[\left[v_j-u_j-\Delta_j\right]_+^{\frac{3}{2}}-\left[u_j-v_j-\Delta_j\right]_+^{\frac{3}{2}}\right]\left(1+\frac{3(1-r)}{2\left(\dot{u}_j^- - \dot{v}_j^-\right)}\left(\dot{u}_j-\dot{v}_j\right)\right) \tag{8}$$

where $k_c = \frac{2E\sqrt{R}}{3(1-\nu^2)}$ is a stiffness coefficient [42], assuming that the impact is between a semi-sphere of radius $R = 0.1[m]$ on each floor of the primary building and a contact point on a flat plane on the core structure, with the contacting bodies made from structural steel and having the same Young's modulus $E = 210[GPa]$ and Poisson's ratio $\nu = 0.3$. Also, $\dot{u}_j^-$ and $\dot{v}_j^-$ are the contact velocities of the *jth* floor and the point of contact on the core, respectively, just before the impact, and r is the coefficient of restitution. The coefficient of restitution of steel-to-steel impacts is typically in the range of 0.6–0.9 [43], and following [44], a value of $r = 0.7$ is adopted in this study for all collisions during the earthquake response. The subscript $(+)$ indicates that only non-negative values of the arguments in the brackets should be taken into account, with zero values being assigned otherwise; this equation models the contacts and separations between the floors of the primary building and the internal core and is a source of strong stiffness nonlinearity in the dynamics of the system, Eq. (7). The Hunt and Crossley contact model considered here (defined in Eq. (8)) uses the work-energy principle in the derivation of the nonlinear hysteresis damping term as a function of the impact penetration and the coefficient of restitution. In addition, in this model, the contact force varies in a nonlinear and continuous manner starting from zero and returning to zero while always remaining compressive only, which is physically reasonable [45]. The Hunt and Crossley formulation has been utilized by many researchers due to its simplicity and straightforward implementation, and it was demonstrated that this model predicts reasonable responses for nearly elastic impact scenarios [46–48].

2.5. Considered earthquakes

The IMTET-based seismic mitigation study was performed by subjecting the structure to the N-S component of the following three historic earthquakes, which were scaled to cause severe seismic excitation to the structure:

i. Kobe – the N-S component recorded at the Kobe Japanese Meteorological Agency (JMA) station during the Hyogo-ken Nanbu earthquake of January 17, 1995.
ii. El Centro – the N-S component recorded at the Imperial Valley Irrigation District substation in El Centro, California, during the Imperial Valley, California earthquake of May 18, 1940.
iii. Northridge – the N-S component recorded at Sylmar County Hospital parking lot in Sylmar, California, during the Northridge, California earthquake of January 17, 1994.

In addition, to test the seismic mitigation efficacy of the IMTET concept under the most severe possible conditions, all seismic records were *time-rescaled* so that the peaks of their response spectra are now located near the fundamental frequency $2\pi/\tilde{T}_1$ of the integrated linear primary building – core system with zero clearance gaps; the rationale here is to ensure that a significant part of the seismic input energy directly excites the fundamental mode of the integrated system, so that a "worst case scenario" is realized. Fig. 5 depicts the acceleration response spectra for the considered ground motions from the three historical earthquakes, and also indicates the leading natural periods of the primary building (T_i), and the zero-gap integrated building-core system ($\tilde{T}_i$). Each of the spectra in Fig. 5 corresponds to a critical viscous

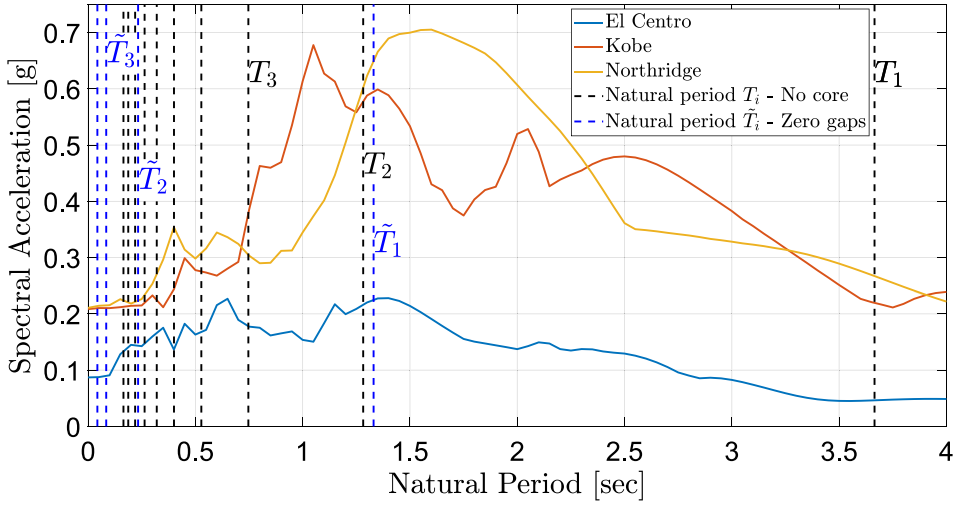

Fig. 5. Seismic ground acceleration response spectra (for viscous damping ratio $\zeta = 0.05$), and leading natural periods of the primary building with no core, T_i, and the zero-gap integrated building-core system, $\tilde{T}_i$.

damping ratio $\zeta = 0.05$.

3. Computational study and IMTET optimization

To explore the effects on seismic mitigation of the nonlinear energy exchanges between the structural modes induced by the vibro-impacts between the floors of the primary structure and the internal core structure, the equations of motion (7) are transformed into modal coordinates through the coordinate transformations $\boldsymbol{u} = \boldsymbol{\Phi_u}\,\boldsymbol{q_u}$ and $\boldsymbol{v} = \boldsymbol{\Phi_v}\,\boldsymbol{q_v}$ expressed in the form,

$$\begin{aligned}
&\boldsymbol{M\Phi_u\ddot{q}_u} + \boldsymbol{C\Phi_u\dot{q}_u} + \boldsymbol{K\Phi_u q_u} - \boldsymbol{f}^{NL}\left(\boldsymbol{\Phi_u\dot{q}_u}, \boldsymbol{\Phi_v\dot{q}_v}, \boldsymbol{\Phi_u q_u}, \boldsymbol{\Phi_v q_v}, \Delta\right) = -\boldsymbol{M\Gamma}\ddot{u}_g \\
&\boldsymbol{M_{cs}\Phi_v\ddot{q}_v} + \boldsymbol{C_{cs}\Phi_v\dot{q}_v} + \boldsymbol{K_{cs}\Phi_v q_v} + \boldsymbol{f}^{NL}\left(\boldsymbol{\Phi_u\dot{q}_u}, \boldsymbol{\Phi_v\dot{q}_v}, \boldsymbol{\Phi_u q_u}, \boldsymbol{\Phi_v q_v}, \Delta\right) = -\boldsymbol{M_{cs}\Gamma}\ddot{u}_g
\end{aligned} \tag{9}$$

where $\boldsymbol{q_u}$ and $\boldsymbol{q_v}$ represent the vectors of the modal amplitudes of the primary and core structures, respectively, and $\boldsymbol{\Phi_u}$ and $\boldsymbol{\Phi_v}$ are the corresponding modal matrices. Pre-multiplying both sides of the first equation in (9) by $\boldsymbol{\Phi}_u^T$ and the second equation by $\boldsymbol{\Phi}_v^T$ yields:

$$\begin{aligned}
&\ddot{\boldsymbol{q}}_u + \widehat{\boldsymbol{C}}\dot{\boldsymbol{q}}_u + \widehat{\boldsymbol{K}}\boldsymbol{q}_u - \boldsymbol{\Phi}_u^T\boldsymbol{f}^{NL} = -\boldsymbol{\Phi}_u^T\boldsymbol{M\Gamma}\ddot{u}_g \\
&\ddot{\boldsymbol{q}}_v + \widehat{\boldsymbol{C}}_{cs}\dot{\boldsymbol{q}}_v + \widehat{\boldsymbol{K}}_{cs}\boldsymbol{q}_v + \boldsymbol{\Phi}_v^T\boldsymbol{f}^{NL} = -\boldsymbol{\Phi}_v^T\boldsymbol{M}_{cs}\boldsymbol{\Gamma}\ddot{u}_g
\end{aligned} \tag{10}$$

Assuming proportional viscous damping guarantees that the resulting transformed damping and stiffness matrices $\widehat{\boldsymbol{C}}$, $\widehat{\boldsymbol{C}}_{cs}$ and $\widehat{\boldsymbol{K}}$, $\widehat{\boldsymbol{K}}_{cs}$, respectively, are diagonal,

$$\begin{aligned}
&\widehat{\boldsymbol{C}} = \boldsymbol{\Phi}_u^T\boldsymbol{C\Phi_u} = \begin{bmatrix} \lambda_{u,1} & & 0 \\ & \ddots & \\ 0 & & \lambda_{u,20} \end{bmatrix},\ \widehat{\boldsymbol{C}}_{cs} = \boldsymbol{\Phi}_v^T\boldsymbol{C}_{cs}\boldsymbol{\Phi_v} = \begin{bmatrix} \lambda_{v,1} & & 0 \\ & \ddots & \\ 0 & & \lambda_{v,20} \end{bmatrix} \\
&\widehat{\boldsymbol{K}} = \boldsymbol{\Phi}_u^T\boldsymbol{K\Phi_u} = \begin{bmatrix} \omega_{u,1}^2 & & 0 \\ & \ddots & \\ 0 & & \omega_{u,20}^2 \end{bmatrix},\ \widehat{\boldsymbol{K}}_{cs} = \boldsymbol{\Phi}_v^T\boldsymbol{K}_{cs}\boldsymbol{\Phi_v} = \begin{bmatrix} \omega_{v,1}^2 & & 0 \\ & \ddots & \\ 0 & & \omega_{v,20}^2 \end{bmatrix}
\end{aligned} \tag{11}$$

where $\omega_{u,\,j}$ and $\omega_{v,\,j}$, represent the *jth* natural frequency of the primary and core structures, respectively, and $\lambda_{u,\,j}$ and $\lambda_{v,\,j}$ are the *jth* modal viscous damping coefficients of the primary and core structures, respectively.

At this point we integrate the first equation in (10) with respect to $\boldsymbol{q_u}$ and the second one with respect to $\boldsymbol{q_v}$ from the time when the ground motion starts, to obtain the following expressions,

$$\begin{aligned}
&\underbrace{\frac{1}{2}\dot{\boldsymbol{q}}_u^T\boldsymbol{I}_{20}\dot{\boldsymbol{q}}_u}_{\triangleq \boldsymbol{E}_k^u} + \underbrace{\int \dot{\boldsymbol{q}}_u^T\widehat{\boldsymbol{C}}\dot{\boldsymbol{q}}_u\boldsymbol{dt}}_{\triangleq \boldsymbol{E}_d^u} + \underbrace{\frac{1}{2}\boldsymbol{q}_u^T\widehat{\boldsymbol{K}}\boldsymbol{q}_u}_{\triangleq \boldsymbol{E}_s^u} - \underbrace{\int \boldsymbol{\Phi}_u^T\boldsymbol{f}^{NL}\dot{\boldsymbol{q}}_u\boldsymbol{dt}}_{\triangleq \boldsymbol{E}_{contacts}^u} = \underbrace{-\int \boldsymbol{\Phi}_u^T\boldsymbol{M\Gamma}\ddot{u}_g\dot{\boldsymbol{q}}_u\boldsymbol{dt}}_{\triangleq \boldsymbol{E}_{input}^u} \\
&\underbrace{\frac{1}{2}\dot{\boldsymbol{q}}_v^T\boldsymbol{I}_{20}\dot{\boldsymbol{q}}_v}_{\triangleq \boldsymbol{E}_k^v} + \underbrace{\int \dot{\boldsymbol{q}}_v^T\widehat{\boldsymbol{C}}_{cs}\dot{\boldsymbol{q}}_v\boldsymbol{dt}}_{\triangleq \boldsymbol{E}_d^v} + \underbrace{\frac{1}{2}\boldsymbol{q}_v^T\widehat{\boldsymbol{K}}_{cs}\boldsymbol{q}_v}_{\triangleq \boldsymbol{E}_s^v} + \underbrace{\int \boldsymbol{\Phi}_v^T\boldsymbol{f}^{NL}\dot{\boldsymbol{q}}_v\boldsymbol{dt}}_{\triangleq \boldsymbol{E}_{contacts}^v} = \underbrace{-\int \boldsymbol{\Phi}_v^T\boldsymbol{M}_{cs}\boldsymbol{\Gamma}\ddot{u}_g\dot{\boldsymbol{q}}_v\boldsymbol{dt}}_{\triangleq \boldsymbol{E}_{input}^v}
\end{aligned} \tag{12}$$

where $\boldsymbol{E_k^{(u,v)}}$, $\boldsymbol{E_d^{(u,v)}}$, $\boldsymbol{E_s^{(u,v)}}$, $\boldsymbol{E_{contacts}^{(u,v)}}$, and $\boldsymbol{E_{input}^{(u,v)}}$ represent the total mass-normalized kinetic, dissipated, strain, contact and seismic input energies, respectively, of the primary (u) and core (v) structures. After simplifications, these instantaneous energies can be rewritten as:

$$\boldsymbol{E}_k^u(\boldsymbol{t}) = \sum_{i=1}^{20}\frac{1}{2}\dot{q}_{u,i}^2(t), \boldsymbol{E}_k^v(\boldsymbol{t}) = \sum_{i=1}^{20}\frac{1}{2}\dot{q}_{v,i}^2(t)$$

$$\boldsymbol{E}_d^u(\boldsymbol{t}) = \sum_{i=1}^{20}\int_0^t \lambda_{u,i}\dot{q}_{u,i}^2 dt, \boldsymbol{E}_d^v(\boldsymbol{t}) = \sum_{i=1}^{20}\int_0^t \lambda_{v,i}\dot{q}_{v,i}^2 dt$$

$$\boldsymbol{E}_s^u(\boldsymbol{t}) = \sum_{i=1}^{20}\frac{1}{2}\omega_{u,i}^2 q_{u,i}^2(t), \boldsymbol{E}_s^v(\boldsymbol{t}) = \sum_{i=1}^{20}\frac{1}{2}\omega_{v,i}^2 q_{v,i}^2(t)$$

$$\begin{aligned}
\boldsymbol{E}_{contacts}^u(\boldsymbol{t}) = &-\sum_{i=1}^{20}\frac{2}{5}\boldsymbol{B}_{u,i}k_c\sum_{j=1}^{20}\left[\left[\boldsymbol{A}_{v,j}\boldsymbol{q_v} - \boldsymbol{A}_{u,j}\boldsymbol{q_u} - \Delta_j\right]_+^{\frac{5}{2}} + \left[\boldsymbol{A}_{u,j}\boldsymbol{q_u} - \boldsymbol{A}_{v,j}\boldsymbol{q_v} - \Delta_j\right]_+^{\frac{5}{2}}\right] \\
&-\sum_{i=1}^{20}\boldsymbol{B}_{u,i}k_c\sum_{j=1}^{20}\int_0^t\left[\left[\boldsymbol{A}_{v,j}\boldsymbol{q_v} - \boldsymbol{A}_{u,j}\boldsymbol{q_u} - \Delta_j\right]_+^{\frac{3}{2}} + \left[\boldsymbol{A}_{u,j}\boldsymbol{q_u} - \boldsymbol{A}_{v,j}\boldsymbol{q_v} - \Delta_j\right]_+^{\frac{3}{2}}\right] \\
&\frac{3(1-r)}{2\left(\boldsymbol{A}_{u,j}\dot{\boldsymbol{q}}_{u,j}^- - \boldsymbol{A}_{v,j}\dot{\boldsymbol{q}}_{v,j}^-\right)}\left(\boldsymbol{A}_{u,j}\dot{\boldsymbol{q}}_{\boldsymbol{u,j}} - \boldsymbol{A}_{v,j}\dot{\boldsymbol{q}}_{\boldsymbol{v,j}}\right)\boldsymbol{A}_{u,j}\dot{\boldsymbol{q}}_{\boldsymbol{u,j}}dt
\end{aligned} \tag{13}$$

$$\begin{aligned}
\boldsymbol{E}_{contacts}^v(\boldsymbol{t}) = &\sum_{i=1}^{20}\frac{2}{5}\boldsymbol{B}_{v,i}k_c\sum_{j=1}^{20}\left[\left[\boldsymbol{A}_{v,j}\boldsymbol{q_v} - \boldsymbol{A}_{u,j}\boldsymbol{q_u} - \Delta_j\right]_+^{\frac{5}{2}} + \left[\boldsymbol{A}_{u,j}\boldsymbol{q_u} - \boldsymbol{A}_{v,j}\boldsymbol{q_v} - \Delta_j\right]_+^{\frac{5}{2}}\right] \\
&+\sum_{i=1}^{20}\boldsymbol{B}_{v,i}k_c\sum_{j=1}^{20}\int_0^t\left[\left[\boldsymbol{A}_{v,j}\boldsymbol{q_v} - \boldsymbol{A}_{u,j}\boldsymbol{q_u} - \Delta_j\right]_+^{\frac{3}{2}} + \left[\boldsymbol{A}_{u,j}\boldsymbol{q_u} - \boldsymbol{A}_{v,j}\boldsymbol{q_v} - \Delta_j\right]_+^{\frac{3}{2}}\right] \\
&\frac{3(1-r)}{2\left(\boldsymbol{A}_{u,j}\dot{\boldsymbol{q}}_{u,j}^- - \boldsymbol{A}_{v,j}\dot{\boldsymbol{q}}_{v,j}^-\right)}\left(\boldsymbol{A}_{u,j}\dot{\boldsymbol{q}}_{\boldsymbol{u,j}} - \boldsymbol{A}_{v,j}\dot{\boldsymbol{q}}_{\boldsymbol{v,j}}\right)\boldsymbol{A}_{v,j}\dot{\boldsymbol{q}}_{\boldsymbol{v,j}}dt
\end{aligned}$$

$$\boldsymbol{E}_{input}^u(\boldsymbol{t}) = -\sum_{i=1}^{20}\int_0^t diag\left(\boldsymbol{\Phi}_u^T\right)_i M_i\ddot{u}_g\dot{q}_{u,i}dt,$$

$$\boldsymbol{E}_{input}^v(\boldsymbol{t}) = -\sum_{i=1}^{20}\int_0^t diag\left(\boldsymbol{\Phi}_v^T\right)_i M_{CS,i}\ddot{u}_g\dot{q}_{v,i}dt$$

$$\boldsymbol{E}_{input}^{tot}(\boldsymbol{t}) = \boldsymbol{E}_{input}^u(\boldsymbol{t}) + \boldsymbol{E}_{input}^v(\boldsymbol{t})$$

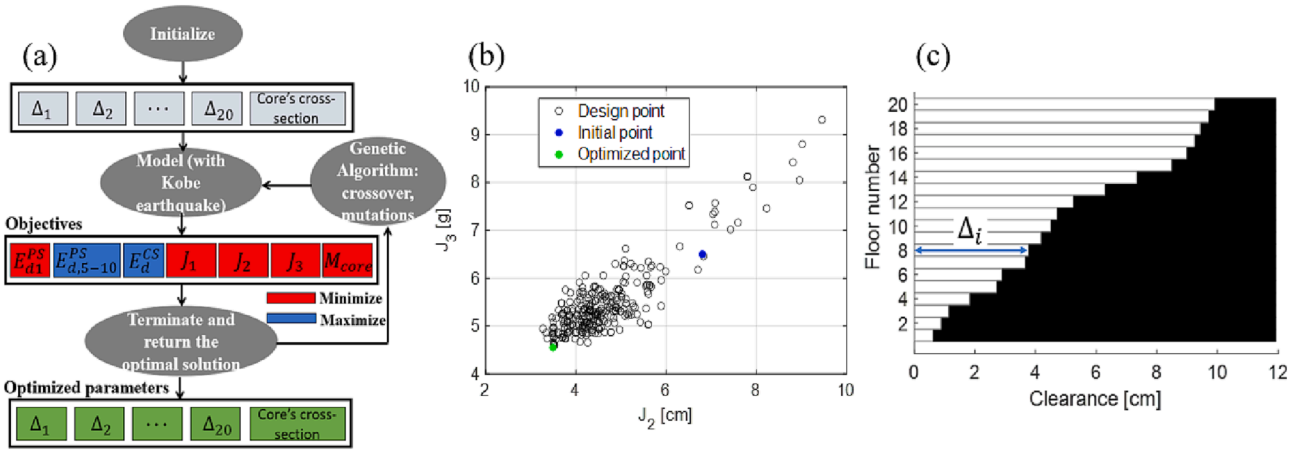

Fig. 6. Optimization of IMTET: (a) Optimization scheme and genetic algorithm, (b) projection of Pareto front in the (J_2,J_3) plane, and (c) optimized distribution of the clearance gaps for the optimized point in (b).

Table 2
Leading objectives for the case of optimized gaps compared to the case of no core structure.

	E_{d1}^{PS} [%]	E_{d5-10}^{PS} [%]	J_1 [m]	J_2 [m]	J_3 [g]	M_{core} [kg]
No core	92.90	~0	1.62	0.14	0.89	–
Optimized gaps	26.17	33.20	0.40	0.035	4.53	2.62×10^5

In Eqs. (13), $q_{u,\ i}(t)$, $q_{v,\ i}(t)$, $\dot{q}_{u,i}(t)$ and $\dot{q}_{v,i}(t)$ denote the modal displacement and velocity of the *ith* mode of the primary building (u) and the core structure (v), respectively. The total seismic input energy imparted into the structural assembly is then represented by $\boldsymbol{E_{input}^{tot}(t)}$. The notations $\boldsymbol{B}_{u,\ i}$ and $\boldsymbol{B}_{v,\ i}$ denote the *ith* rows of the matrices $\boldsymbol{\Phi}_u^T$ and $\boldsymbol{\Phi}_v^T$, respectively. Finally, $\boldsymbol{A}_{u,\ j}$ and $\boldsymbol{A}_{v,\ j}$ represent the *jth* rows of the matrices $\boldsymbol{\Phi_u}$ and $\boldsymbol{\Phi_v}$, respectively.

Having defined the previous energy measures, we are now in position to study the efficacy of the IMTET concept to passively mitigate the seismic response of the primary building, and also to quantify the "utilization" of the intrinsic modal dissipative capacity of the building itself. To this end, a multi-task optimization procedure using a multi-objective genetic algorithm (MOGA) was employed to determine the optimal values of the clearance distributions $\boldsymbol{\Delta} = [\Delta_1,\ \cdots,\ \Delta_{20}]^T$ as well as the core structure cross-section dimensions. Following Fig. 3b, the core was designed as a linearly tapered steel structure extended along the entire height of the 20-story structure, and its variable thickness was defined using a linear variation between the largest and smallest thicknesses, i.e., the thicknesses of the first and last floors, respectively. In the optimization procedure, the optimal values of the largest and smallest thicknesses of the core structure were determined.

The uniqueness of this algorithm lies in its ability to avoid converging to local solutions and find global optima in the search space. The optimization process is shown in Fig. 6a. First an initial population is set and used for the radial basis functions, which are real-valued functions that depend only on the Euclidean distance between an interpolation point and any variable field point, which are used as interpolants. Thereafter, values of the objective functions for the initial population are calculated, and radial basis response surfaces are created based on the simulations yielding new design points. Next, the genetic algorithm is run and generates a new population via selection, crossover, and mutation in which the radial basis is used as an evaluator to measure the error for each design point. If the error for a generated point is acceptable, it is included in the next population to be run through the MOGA algorithm. If the error is not acceptable, the point is used as a new design point for the radial basis construction. Finally, MOGA converges when the maximum allowable Pareto percentage has been achieved, resulting in the optimized values as the output. If convergence does not occur, the process is repeated from generating a new population up to the maximum number of iterations.

The aim of the optimization is, through a practical design, to maximize the low-to-high frequency IMTET through nonlinear modal energy redistribution caused by the vibro-impacts, while keeping the response of the primary building as small as possible. This is achieved by imposing *seven objectives*, namely, (i) minimize the percentage of seismic input energy, $E_{d1}^{PS} = \int_0^{t_d} \lambda_{u,1}\dot{q}_{u,1}^2 dt / E_{input}^{tot}(t_d)$, dissipated by the first mode of the primary building for the duration of the earthquake, where t_d denotes the total duration of the earthquake record; (ii) maximize the percentage of input energy, $E_{d5-10}^{PS} = \sum_{i=5}^{10} \int_0^{t_d} \lambda_{u,i}\dot{q}_{u,i}^2 dt / E_{input}^{tot}(t_d)$,

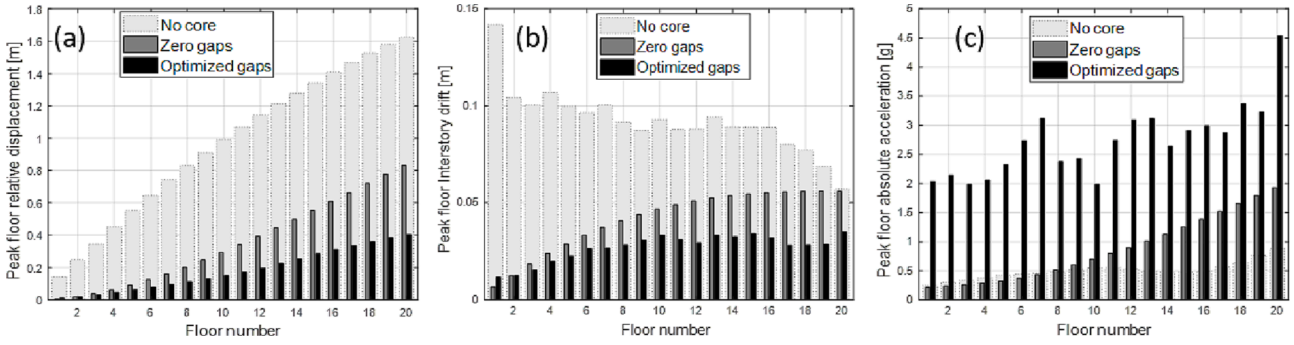

Fig. 7. Comparison of building response with core and optimized gaps, without core, and with core and zero gaps, subject to the Kobe earthquake: (a) Peak floor relative displacement, (b) Peak floor inter-story drift, and (c) Peak floor absolute acceleration.

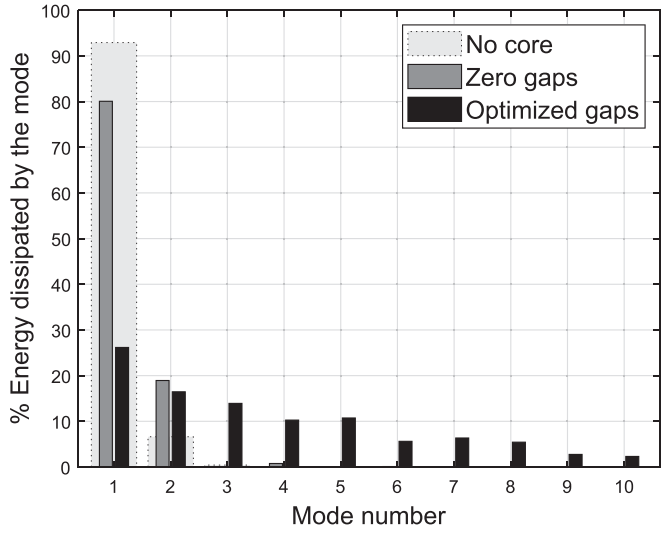

Fig. 8. Percentage of seismic input energy dissipated by the inherent damping of the leading modes of the primary building, with low to high frequency IMTET occurring for the case of optimized gaps; note that the responses for the cases of zero gaps and optimized gaps are projected onto the modal space of the no core building.

dissipated by modes 5 to 10 of the primary building; (iii) maximize the percentage of the seismic input energy, $E_d^{CS} = \sum_{i=1}^{20} \int_0^{t_d} \lambda_{v,i} \dot{q}_{v,i}^2 dt / E_{input}^{tot}(t_d)$, dissipated by the modes of the core structure; (iv) minimize the maximum peak floor relative displacement with respect to ground, $J_1 = max\,(|u_j(t)|)$, $j \in [1, \cdots, 20]$; (v) minimize the maximum inter-story drift, $J_2 = max\,(|d_j(t)|)$, where $d_j(t)$ is the *jth* inter-story drift; (vi) minimize the maximum peak floor absolute acceleration with respect to ground, $J_3 = max\left(\left|\ddot{u}_j(t) + \ddot{u}_g\right|\right)$; and (vii) minimize the total mass of the core structure, M_{core} (for practical considerations).

The optimization was performed for the Kobe historical earthquake only (a rather severe case of seismic excitation due to its highest energy content and destructive capacity), whereas the robustness of the optimized design was later established by applying the other two historical earthquakes to the optimized design (derived based on Kobe excitation). The initiation point was an arbitrary clearance distribution – blue circle in Fig. 6b, and a total of 100 iterations were carried out to form a Pareto front (see projection in Fig. 6b), from which the optimization point was selected – green circle in that Figure. It can be concluded from Table 2 that for the optimized clearance distribution (shown in Fig. 6c), only a small portion of the net seismic input energy was dissipated by the fundamental structural mode, compared to the case without the core, while a more significant portion of the seismic input energy is eventually dissipated by higher structural modes, yielding drastic suppression of floor relative displacements and inter-story drifts. However, it should be noted that this excellent performance comes at the cost of a moderate increase in floor acceleration levels caused by the impacts between the floors and core structure, although the durations of these impacts are extremely short and therefore the possibility of damage decreases accordingly. In the optimized design shown in Fig. 6 the optimum design of the core structure has just 5% of the building mass. The following computational results provide a preliminary demonstration of the effectiveness and robustness of the optimized design of Fig. 6. As such, they can be regarded as a first step towards practical implementation of IMTET for rapid seismic mitigation of the primary building response subjected to the severe earthquake ground motion.

4. Results and discussion

Numerical results are given below to demonstrate the effectiveness of the IMTET concept for rapid and effective seismic mitigation of the primary building response. For comparison, the seismic response for three different structural configurations are considered for the 20-story building: (i) with no internal core structure, (ii) with an internal core and optimal clearance gaps (see Fig. 6), and (iii) with an internal core and zero gaps (zero-gap integrated building-core system). Configurations (i) and (iii) have linear dynamics as there are no impacts, whereas (iii) has strongly nonlinear dynamics and is designed for optimal IMTET. Case (iii) – zero gaps – is presented in order to prove that the drastic improvement in seismic mitigation in case (ii) is due to the vibro-impacts and fast-scale IMTET.

The results in Fig. 7 verify the extremely effective attenuation of the structural response for the nonlinear case with optimized core and clearance gaps, compared to the linear cases of no core and zero-gap core. Drastic reductions of the peak floor displacement responses relative to the ground (Fig. 7a) and peak floor inter-story drifts (Fig. 7b) are found. The peak floor absolute accelerations increase (Fig. 7c) but remain within a range of similar order of magnitude compared to the linear case of zero gaps.

The governing nonlinear mechanism responsible for the drastic enhancement in seismic mitigation is shown in Fig. 8, where the percentage of seismic input energy eventually dissipated by the inherent

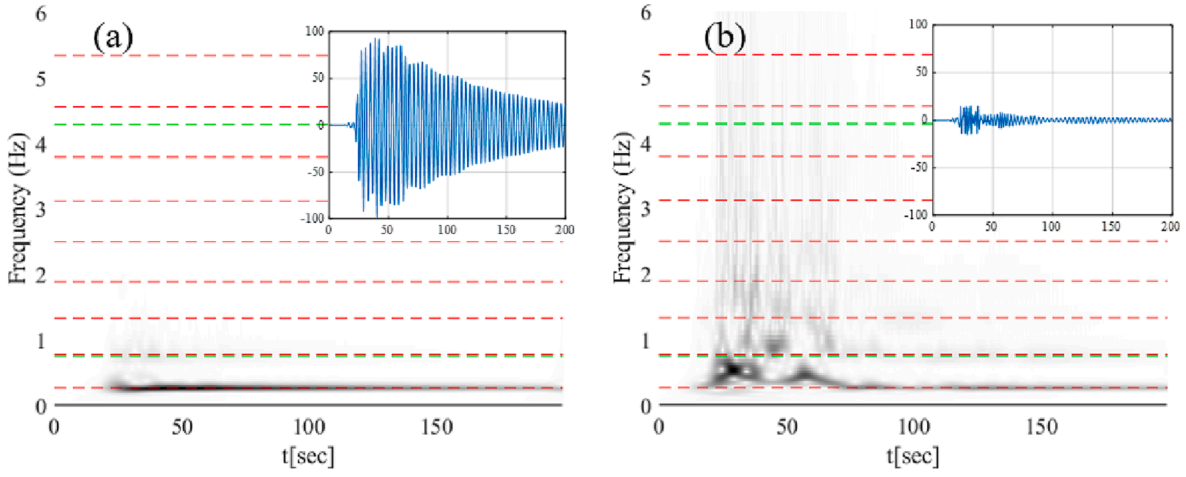

Fig. 9. Wavelet spectra of the 10*th* floor displacements (shown in the insets in [cm]) for the Kobe earthquake: Case of (a) no core, and (b) core with optimized gaps – dashed lines denote the natural frequencies of the building with no core; note that in the nonlinear case (core with optimized gaps) effective mitigation starts right from the first response cycle.

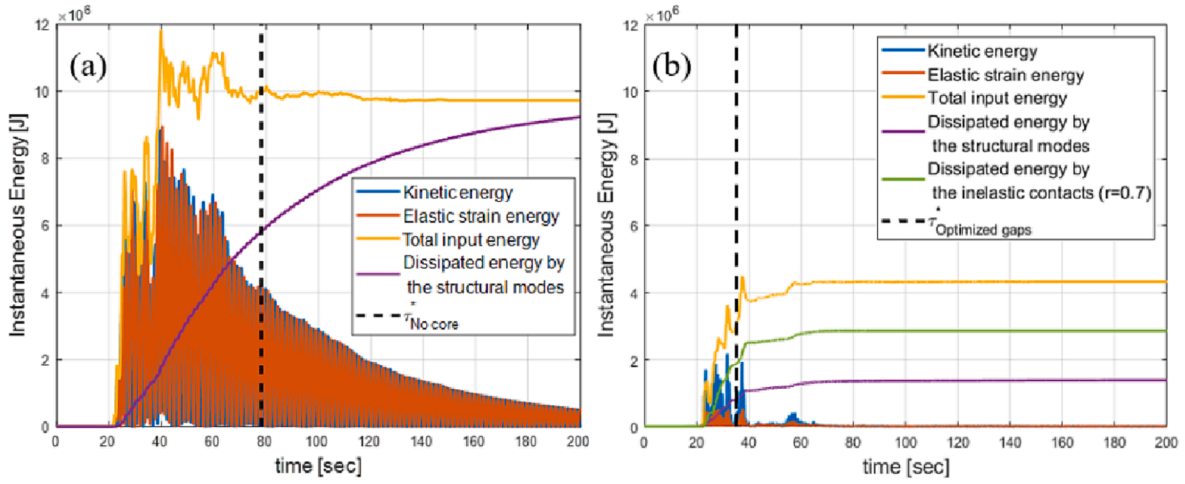

Fig. 10. Instantaneous kinetic and potential energies, cumulative dissipated energy, and total seismic input energy for the system with (a) no core – linear system, and (b) optimized core gaps – nonlinear system; note the drastic reduction of seismic input energy in (b).

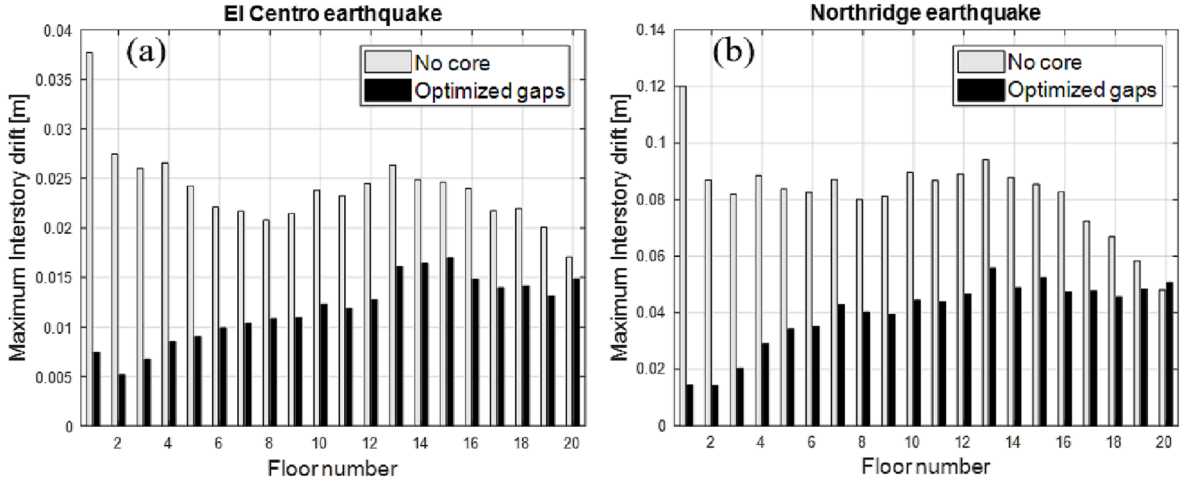

Fig. 11. Maximum inter-story drift of the 20-story building with no core, and core with optimized gaps: (a) El Centro and (b) Northridge earthquakes.

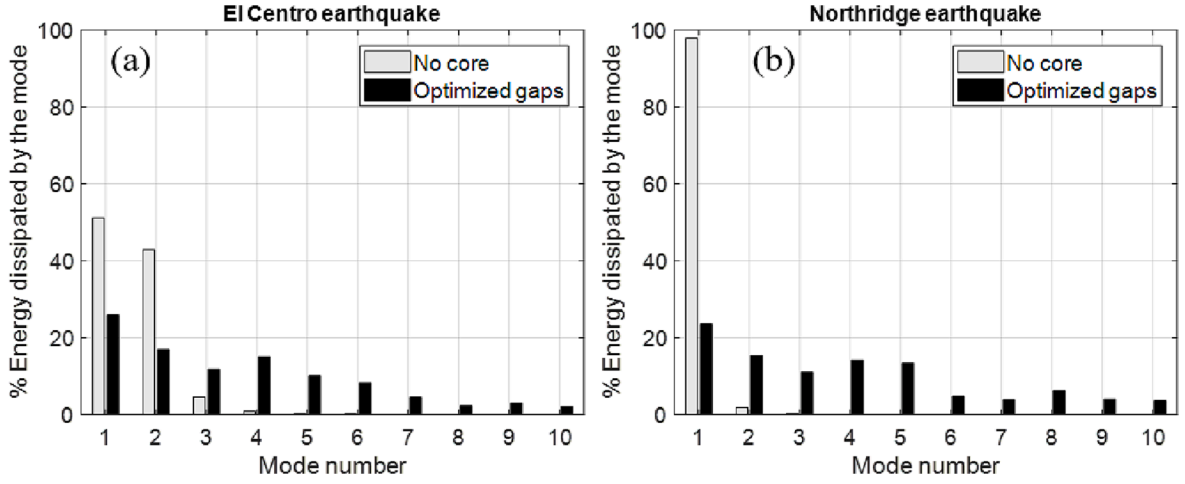

Fig. 12. Seismic input energy (%) dissipated by the inherent damping of the leading modes of the building with no core and core with optimized gaps: (a) El Centro and (b) Northridge earthquakes; for the case of optimized gaps a portion of the seismic energy is also dissipated by inelastic impacts.

(modal) damping of each of the ten leading structural modes of the primary building (with no core) is depicted. Indeed, compared to the linear cases of no core – where the energy dissipation is dominated by the fundamental structural mode which eventually dissipates as much as ~88% of the seismic input energy, and zero-gap core where again a few low-frequency modes dissipate the seismic input energy, in the case of

the optimized clearance gaps as many as eight leading modes effectively participate in the seismic input energy dissipation. Hence, for the structure with optimized gaps, there is a rapid and irreversible nonlinear targeted energy transfer (or IMTET) from the low structural modes to the higher ones, causing rapid reduction of the structural response (see Figs. 7a-b). In fact, the impacts between the floors and the core cause rapid "modal energy redistribution" from low to high frequency modes, as well as better "utilization" of the inherent dissipative capacity of the primary building itself, because more of its modes now participate in the task of dissipating the seismic input energy. This process is as if the inherent dissipative modal capacity of the building is being "activated" by the nonlinear impacts. Note that, apart from rapid IMTET, the optimized core structure also promotes strong dissipation of seismic energy due to intense inelastic impacts at the early, high-energy stage of the response.

The rapid low-to-high nonlinear transfer of seismic energy due to IMTET in the building with the optimized internal core structure is clearly shown in the wavelet spectra of Figs. 9a,b; in fact, from the corresponding 10*th* floor displacements [in cm] shown in the insets, it is clear that extremely effective and rapid seismic suppression starts right from the first half-cycle of the response. This is exclusively due to the non-resonant IMTET mechanism caused by the Hertzian impacts that occur at sufficiently fast time scale to prevent resonances from being excited in the structure (as these typically occur on much slower time scales – the process of resonance takes time to build up).

The absence of nonlinear resonance with structural modes is clearly evidenced in the wavelet spectrum of Fig. 9b, where localized (in time) frequency "bursts" are realized at the time instants of the impacts, especially in the initial, highly energetic and strongly nonlinear regime of the response. On the contrary, in the wavelet spectrum of Fig. 9a, resonant excitation of the fundamental structural mode in the system with no core is realized – as evidenced by the "locked" dominant harmonic of the response at the first natural frequency; this is to be expected, because the Kobe earthquake is scaled (in time) precisely to excite in resonance the fundamental mode of the building with zero gap core. Hence, *IMTET is a non-resonant nonlinear energy transfer mechanism, which relies on rapid energy scattering to high modal frequencies due to short-duration vibro-impacts*.

A rather non-intuitive, additional finding related to the IMTET-based optimal design is illustrated in Fig. 10 where the instantaneous kinetic and potential energies of the primary building (Figs. 10a,b), and the cumulative dissipated energies and seismic input energies for the primary building without (Fig. 10a) and with optimized core (Fig. 10b), are depicted. In the same plots the characteristic times are shown for comparison (defined as the time for the input energy to drop to e^{-1} of its net value). Clearly, *the nonlinear effects of the impacts between the floors and the core reduce the seismic input energy to the integrated building-core system by nearly 60% compared with the no core case.* Hence, apart from IMTET, the strongly nonlinear impacts drastically reduce the overall seismic energy input into the system providing, in essence, an effective nonlinear stiffening of the integrated system (or an effective impedance increase at the point of entry of the seismic energy). This suggests that it is possible to drastically decrease the seismic input energy into the primary building by augmenting it with local internal nonlinearities.

Lastly, it is necessary to test the robustness of the optimized clearance gap design of Fig. 6c based on the severe Kobe earthquake, which was time-rescaled to achieve a most challenging excitation scenario as it excited in resonance the fundamental mode of the primary building (see Fig. 8). Nevertheless, it is necessary to study how the optimized design performs with two other historic seismic excitations, and this is shown in Fig. 11 for the maximum inter-story drifts, and Fig. 12 for the modal energy dissipations. For comparison, the corresponding responses of the primary building with no internal core are also shown. The persistence of strong IMTET for the historical earthquakes is shown by these results, as evidenced by the drastic reduction in the inter-story drifts for the nonlinear case, and the uniformly low-to-high modal energy scattering of the seismic input energy for all excitation scenarios. These results highlight the robustness of the optimized IMTET design.

5. Concluding remarks

In this paper, a new concept for seismic mitigation is presented, and its efficacy demonstrated using a benchmark model of a twenty-story steel building structure. The approach is based on an extremely rapid nonlinear scattering of the seismic input energy from low to high frequency modes of the building through strong local nonlinearities, which is referred to as intermodal targeted energy transfer (IMTET). The IMTET-based seismic mitigation study was performed using the N-S components of three historical earthquakes: Kobe (1995), El Centro (1940), and Northridge (1994), which were time-scaled to cause severe seismic excitation of the model building structure.

Prior to the demonstration of the IMTET concept, a reduced order model of 20 DOFs was developed for the considered building, maintaining the important dynamics of the full model. Then, an internal core structure was introduced with a specified clearance distribution between the floor slabs and the core structure along the height of the building, thus inducing vibro-impact nonlinearities in the transient dynamics. The interactions between the primary structure and the internal core structure were modeled as dissipative Hertzian contacts.

To study the efficacy of the IMTET concept for effective and robust passive seismic mitigation, quantification of the "utilization" of the intrinsic modal dissipative capacity of the structure is required. To this end, a multi-task optimization procedure using a multi-objective genetic algorithm (MOGA) was employed to determine the optimal values of the clearance distribution between the primary and the core structure, as well as the core structure cross-section dimensions. The aim of the optimization was to maximize the low-to-high frequency IMTET through nonlinear modal energy redistribution caused by the vibro-impacts, while keeping the amplitude of the response of the building as small as possible and respecting practical design considerations. The optimization was performed for the Kobe earthquake excitation, which has the highest energy content and hence represents a rather severe excitation scenario. Then, the robustness of the optimized IMTET design to changes in seismic input was demonstrated.

It was shown that for the nonlinear case with optimized gaps there is a significant improvement in seismic mitigation due to the vibro-impacts compared to the two linear cases, namely, the systems with no core and zero clearance gaps. The potential to direct a significant portion of the seismic input energy from low to high frequency modes was demonstrated; as a result, the response of the primary structure is reduced substantially (a reduction of 75% in the maximum peak floor displacement response relative to the ground, and approximately 90% reduction in the maximum inter-story drift with respect to the no core case), because higher structural modes generally exhibit lower amplitudes of vibration and dissipate energy more efficiently. Thus, the dissipative capacity of the system itself is enhanced. In addition, at the time at which vibro-impacts occur, energy is also dissipated due to the inelastic Hertzian contacts, which has been shown to be a very efficient mechanism for energy dissipation.

The strong nonlinear mechanism of vibro-impacts resulted in a significant reduction of the maximum levels of seismic response of the primary building, which is essential for effective seismic protection. Because such fast-scale IMTET cannot be realized with TET-based resonance mechanisms, one concludes that the discontinuous nature of the vibro-impacts is the key to the success of the IMTET-based seismic mitigation design proposed in this paper.

Author statement

The authors declare that this manuscript is original, has not been published before and is not currently being considered for publication elsewhere.

Declaration of Competing Interest

The authors declare that they have no conflict of interest.

Data availability

Data will be made available on request.

Acknowledgements

The authors are grateful to the Israel Science Foundation (Grant No. 2598/21) for financial support.

Appendix A. : Mass (in $[kg]$ **[kg]**) and stiffness (in $\left[N/m\right]$) matrices for the reduced order model of the 20-story primary structure.

$$M_{20\times20} = \begin{bmatrix}
286774.9 & -446.79 & -730.25 & 370.62 & -59.10 & 13.95 & 19.14 & 14.64 & 9.49 & 3.91 & -3.99 & 5.51 & -2.91 & -7.75 & 3.37 & -8.92 & -25.49 & -28.74 & -34.80 & -103.82 \\
 & 278301.8 & 1514.08 & -1674.81 & 426.68 & 35.67 & 0.02 & 8.15 & 4.42 & 1.77 & -1.58 & 2.50 & -1.18 & -3.26 & 1.53 & -3.82 & -11.00 & -12.42 & -15.07 & -44.87 \\
 & & 277047.7 & 1724.98 & -855.91 & -69.52 & 40.66 & 5.69 & 7.31 & 3.50 & -1.88 & 4.48 & -1.49 & -4.70 & 2.76 & -5.84 & -17.16 & -19.47 & -23.83 & -70.41 \\
 & & & 277158.2 & 163.48 & -468.66 & 202.80 & -29.98 & 3.99 & 3.97 & -1.13 & 4.06 & -0.90 & -3.43 & 2.51 & -4.56 & -13.71 & -15.62 & -19.28 & -56.56 \\
 & & & & 275702.9 & 1065.54 & -1086.15 & 263.46 & 29.96 & -0.90 & 0.40 & 5.73 & -0.81 & -3.93 & 3.51 & -5.62 & -17.25 & -19.73 & -24.55 & -71.52 \\
 & & & & & 274679.1 & 1255.52 & -619.37 & -57.21 & 27.67 & -3.66 & 7.13 & -0.06 & -3.46 & 4.60 & -5.85 & -18.74 & -21.62 & -27.31 & -78.51 \\
 & & & & & & 274859.6 & 264.48 & -479.59 & 201.96 & -39.52 & 4.99 & 0.89 & -3.00 & 4.74 & -5.42 & -17.79 & -20.61 & -26.2 & -74.90 \\
 & & & & & & & 275357.5 & 1053.32 & -1086.26 & 253.14 & 26.92 & -3.31 & -0.61 & 5.77 & -4.81 & -17.04 & -20.02 & -26.11 & -73.00 \\
 & & & & & & & & 274698.6 & 1237.64 & -632.55 & -54.13 & 22.27 & -3.15 & 6.67 & -3.57 & -14.93 & -17.95 & -24.34 & -65.79 \\
 & & & & & & & & & 274777.2 & 233.33 & -435.51 & 168.38 & -30.13 & 4.43 & -0.86 & -8.147 & -10.26 & -15.08 & -38.04 \\
 & & & & & & & & & & 274196 & 917.53 & -967.08 & 222.68 & 18.02 & -0.93 & -1.126 & -3.12 & -7.13 & -12.58 \\
 & & & & & & & & & & & 273540.3 & 1088.38 & -588.57 & -36.72 & 10.32 & -12.09 & -13.62 & -20.91 & -50.47 \\
 & & & & & & & & & & & & 273460.3 & 193.07 & -297.00 & 91.19 & -15.55 & -2.85 & -5.80 & -8.00 \\
 & & & & & & & & & & & & & 272345.9 & 642.27 & -609.79 & 124.99 & 11.67 & -3.74 & 7.83 \\
 & & & & & & & & & & & & & & 271719.7 & 774.67 & -423.02 & -54.46 & -10.73 & -35.83 \\
 & & & & & & & & & & & & & & & 271743 & 241.45 & -386.93 & 99.48 & 36.21 \\
 & & & & & & & & & & & & & & & & 271079.2 & 886.48 & -494.05 & 91.09 \\
 & & & & & & & & & & & & & & & & & 270806.8 & -99.41 & 20.80 \\
 & & & & & & & & & & & & & & & & & & 271126.2 & -1205.18 \\
 & & & & & & & & & & & & & & & & & & & 284471.7
\end{bmatrix}$$

Symmetric

$$K_{20\times20} = \begin{bmatrix}
877436471 & -583588215 & 158747840 & -32412952 & 5556070 & 258940.5 & -29773.7 & 23701.5 & 25495.67 & 16126.02 & 25458.52 & 14885.91 & 15134.08 & 21334.31 & 9690.586 & 13108.49 & 25202.12 & 25450.69 & 23883.81 & 89365.33 \\
 & 1182285736 & -814125668 & 248893013 & -42154686 & -1713426 & 304965.1 & -38107.9 & 8523.142 & 7527.733 & 11053.81 & 6508.902 & 6521.506 & 9333.245 & 4195.71 & 5734.603 & 11025.21 & 11133.97 & 10448.51 & 39094.83 \\
 & & 1303913117 & -880840179 & 217972120 & 8905765 & -1518404 & 243020.3 & 30288.91 & 9308.841 & 18438.63 & 10601.63 & 10759.55 & 15171.87 & 6820.177 & 9321.724 & 17921.74 & 18098.53 & 16984.29 & 63549.55 \\
 & & & 1256216992 & -663892525 & 85333778 & -14446054 & 2173993 & 130129.9 & -10653.6 & 18162.83 & 8951.038 & 8927.111 & 12623.88 & 5673.306 & 7754.188 & 14908.1 & 15055.13 & 14128.25 & 52859.27 \\
 & & & & 905230115 & -538161378 & 136072449 & -20187691 & -1047227 & 197608.7 & -8615.4 & 10158.1 & 11896.61 & 16416.39 & 7394.014 & 10108.5 & 19434.12 & 19625.76 & 18417.46 & 68912.27 \\
 & & & & & 893949470 & -580107187 & 125619291 & 6578697 & -1106674 & 192190.6 & 21244.19 & 12252.91 & 19359.38 & 8619.233 & 11770.05 & 22630.84 & 22853.97 & 21446.97 & 80247.33 \\
 & & & & & & 910420871 & -525323245 & 86763840 & -14664448 & 2223539 & 115180.2 & -3944.92 & 21374.81 & 8541.177 & 11539.9 & 22211.79 & 22429.44 & 21048.56 & 78756.26 \\
 & & & & & & & 839194800 & -536527281 & 135631844 & -20135276 & -917041 & 169288.5 & -3075.22 & 8187.131 & 12375 & 23565.47 & 23812.04 & 22346.89 & 83613.47 \\
 & & & & & & & & 892048987 & -578689079 & 125568636 & 5783664 & -934456 & 160062.1 & 13952.52 & 11909.43 & 24241.5 & 24399.33 & 22893.08 & 85659.13 \\
 & & & & & & & & & 888477415 & -490432260 & 70067478 & -11368051 & 1673361 & 63080.23 & 1481.267 & 18546.93 & 17787.94 & 16643.69 & 62296.88 \\
 & & & & & & & & & & 738338620 & -449703042 & 109610718 & -15868833 & -533273 & 79629.26 & 4263.151 & 13168.25 & 12821.25 & 47748.48 \\
 & & & & & & & & & & & 751461379 & -482800065 & 102644262 & 3481394 & -448881 & 84780.07 & 29570.76 & 24829.67 & 94290.98 \\
 & & & & & & & & & & & & 732235816 & -381432162 & 38807539 & -5114135 & 652295.7 & 43563.5 & 8915.485 & 48449.67 \\
 & & & & & & & & & & & & & 539328034 & -298246122 & 59148905 & -7324099 & -325965 & 60900.56 & 55000.07 \\
 & & & & & & & & & & & & & & 513833938 & -318159391 & 58135508 & 2734487 & -332828 & 116397.7 \\
 & & & & & & & & & & & & & & & 517694947 & -288047940 & 40329697 & -5463368 & -123141 \\
 & & & & & & & & & & & & & & & & 462289014 & -284787408 & 57084518 & 1692601 \\
 & & & & & & & & & & & & & & & & & 449091595 & -228053617 & 20707320 \\
 & & & & & & & & & & & & & & & & & & 289015341 & -112571659 \\
 & & & & & & & & & & & & & & & & & & & 89169474
\end{bmatrix}$$

Symmetric

References

[1] Uang CM, Bertero VV. Use of energy as a design criterion in earthquake-resistant design. In: Report No. UCB/EERC-88/18, Berkeley, Calif.: Earthquake Engineering Research Center. University of California; 1988.

[2] Housner GW, Bergman LA, Caughey TK, Chassiakos AG, Claus RO, Masri SF, et al. Structural control: past, present and future. ASCE J Eng Mech 1997;123(9): 897–971.

[3] Buckle IG, Mayes RL. Seismic isolation history, application, and performance–a would view. Earthq Spectra 1990;6(2):161–201.

[4] Mayes RL, Sveinsson BI, Buckle IG. Seismic isolation: an economic rehabilitation alternative. Construct Spec 1987:76–92.

[5] Walters M, Elsesser E, Allen EW. Base isolation of the existing City and County Building in Salt Lake City. In: Proceedings of a Seminar on Base Isolation and Passive Energy Dissipation. Applied Technology Council; 1986. Report No. 17.

[6] Soong TT, Constantinou MC. Passive and active structural vibration control in civil engineering. New York: Springer-Verlag Wien; 1994.

[7] Saitoh M. An external rotary friction device for displacement mitigation in base isolation systems. Struct Control Health Monit 2014;21(2):173–88.
[8] Nepal S, Saitoh M. Improving the performance of conventional base isolation systems by an external variable negative stiffness device under near-fault and long-period ground motions. Earthq Eng Eng Vib 2020;19:985–1003.
[9] Soong TT, Spencer BF. Supplemental energy dissipation: state-of-the-art and state of-the-practice. Eng Struct 2002;24:243–59.
[10] De Domenico D, Ricciardi G, Takewaki I. Design strategies of viscous dampers for seismic protection of building structures: A review. Soil Dyn Earthq Eng 2019;118: 144–65.
[11] Clark AJ. Multiple passive tuned mass dampers for reducing earthquake induced building motion. In: Proc., 9th World Conf. on Earthquake Engineering. 5; 1988. p. 779–84.
[12] Den Hartog JP. Mechanical vibrations. New York: McGraw-Hill, Inc; 1947.
[13] Koshimura K, Tatsumi M, Hata K. Vibration control of the main towers of the Akashi Kaikyo Bridge. In: Proc., First World Conf. on Struct. Control. 2; 1994. TP3 98–106.
[14] Miranda JC. On tuned mass dampers for reducing the seismic response of structures. Earthq Eng Struct Dyn 2005;34(7):847–65.
[15] Miyamoto HK, Gilani ASJ, Garza J, Mahin SA. Seismic retrofit of a landmark structure using a mass damper. In: Improving the seismic performance of existing buildings and other structures; 2009.
[16] Tributsch A, Adam C. Evaluation and analytical approximation of tuned mass damper performance in an earthquake environment. Smart Struct Syst 2012;10(2): 155–79.
[17] Balendra T, Wang CM, Cheong HF. Effectiveness of tuned liquid column dampers for vibration control of towers. Eng Struct 1995;17(9):668–75.
[18] Fujino Y, Pacheco BM, Chaiseri P, Sun LM. Parametric studies on tuned liquid damper (TLD) using circular containers by free oscillation experiments. Struct Eng Earthq Eng JSCE 1988;5(2):381–91.
[19] Sun LM, Fujino Y, Koga K. A model of tuned liquid damper for suppressing pitching motions of structures. Earthq Engrg Struct Dyn 1995;24:625–36.
[20] Xu YL, Samali B, Kwok KCS. Control of along wind response of structures by mass and liquid dampers. J Engrg Mech ASCE 1992;118(1):20–39.
[21] Mahmoodi P, Robertson LE, Yontar M, Moy C, Feld I. Performance of viscoelastic dampers in world trade center towers. In: Dynamic of structures, structures congress '87. Orlando: FL; 1987.
[22] Tsampras G, Sause R, Zhang D, Fleischman RB, Restrepo JI, Mar D, et al. Development of deformable connection for earthquake-resistant buildings to reduce floor accelerations and force responses. Earthq Eng Struct Dyn 2016;45: 1473–94.
[23] Tsampras G, Sause R, Fleischman RB, Restrepo JI. Experimental study of deformable connection consisting of buckling-restrained brace and rubber bearings to connect floor system to lateral force resisting system. Earthq Eng Struct Dyn 2017;2017(46):1287–305.
[24] Vakakis AF, Gendelman OV, Bergman LA, McFarland DM, Kerschen G, Lee YS. Nonlinear targeted energy transfer in mechanical and structural systemsvol. I and II. Dordrecht: Solid Mechanics and Its Applications, Springer; 2008.
[25] Gendelman OV. Transition of energy to a nonlinear localized mode in a highly asymmetric system of two oscillators. Nonlin Dyn 2001:237–53.
[26] Gendelman OV, Manevitch LI, Vakakis AF, McCloskey.. Energy pumping in nonlinear mechanical oscillators: Part I – Dynamics of the underlying Hamiltonian systems. ASME J Appl Mech 2001;68:34–41.
[27] Vakakis AF, Genderman OG. Energy pumping in nonlinear mechanical oscillators: part II – resonance capture. ASME J Appl Mech 2001;68:42–8.
[28] Gendelman OV, Gorlov DV, Manevitch LI, Musienko AI. Dynamics of coupled linear and essentially nonlinear oscillators with substantially different masses. J Sound Vib 2005;286:1–19.
[29] Gourdon E, Alexander NA, Taylor CA, Lamarque CH, Pernot S. Nonlinear energy pumping under transient forcing with strongly nonlinear coupling: theoretical and experimental results. J Sound Vib 2007;300(3–5):522–51.
[30] Gourdon E, Lamarque CH. Nonlinear energy sinks with uncertain parameters. ASME J Nonlinear Comput Dyn 2006;1:187–95.
[31] Luo J, Wierschem NE, Hubbard SA, Fahnestock LA, Quinn DD, McFarland DM, et al. Large-scale experimental evaluation and numerical simulation of a system of nonlinear energy sinks for seismic mitigation. Eng Struct 2014;77:34–48.
[32] Wierschem NE, Hubbard SA, Luo J, Fahnestock LA, Spencer BF, McFarland DM, et al. Response attenuation in a large-scale structure subjected to blast excitation utilizing a system of essentially nonlinear vibration absorbers. J Sound Vib 2017; 389:52–72.
[33] Luo J, Wierschem NE, Fahnestock LA, Spencer BF, Quinn DD, McFarland DM, et al. Design, simulation, and large-scale testing of an innovative vibration mitigation device employing essentially nonlinear elastomeric springs. Earthq Eng Str Dyn 2014;43(12):1829–51.
[34] AL-Shudeifat MA, Vakakis AF, Bergman LA. Shock mitigation by means of low-to high frequency nonlinear targeted energy transfers in a large scale structure. J Comp Nonl Dyn 2016;11(2).
[35] Vakakis AF, Gendelman OV, Bergman LA, Mojahed A, Gzal M. Nonlinear targeted energy transfer: state of the art and new perspectives. Nonlinear Dyn 2022;108: 711–41.
[36] Gzal M, Fang B, Vakakis AF, Bergman LA, Gendelman OV. Rapid non-resonant intermodal targeted energy transfer (IMTET) due to Vibro-impact nonlinearity. Nonlin Dyn 2020;101:2087–106.
[37] Gzal M, Vakakis AF, Bergman LA, Gendelman OV. Extreme intermodal energy transfers through vibro-impacts for highly effective and rapid blast mitigation. Commun Nonlinear Sci Num Simulat 2021;103(106012):1–13.
[38] Tempelman JR, Mojahed A, Gzal M, Matlack KH, Gendelman OV, Bergman LA, et al. Experimental inter-modal targeted energy transfer in a cantilever beam undergoing Vibro-impacts. J Sound Vib 2022;539:117212.
[39] Spencer Jr BF, Christenson RE, Dyke SJ. Next generation benchmark control problems for seismically excited buildings. In: Kobori T, et al., editors. Proc., 2nd World Conf. on Structural Control. 2. Wiley; 1999. p. 1135–360.
[40] Wilson EL, Penzien J. Evaluation of orthogonal damping matrices. Int J Numer Methods Eng 1972;4(1):5–10.
[41] Craig Jr RR. Structural dynamics. In: An Introduction to Computer Methods. New York: John Wiley & Sons; 1981.
[42] Hunt KH, Crossley FRE. Coefficient of restitution interpreted as damping in vibro-impact. J Appl Mech 1975;7:440–5.
[43] Goldsmith W. Impact-theory and physical behaviour of colliding solids. London: Edward Arnold (Publishers) Ltd.; 1960.
[44] Jankowski R. Experimental study on earthquake-induced pounding between structural elements made of different building materials. Earthq Eng Struct Dyn 2010;39:343–54.
[45] Flores P, Lankarani HM. Contact force models for multibody dynamics. Switzerland: Springer International Publishing; 2016.
[46] Marhefka DW, Orin DE. A compliant contact model with nonlinear damping for simulation of robotic systems. IEEE Trans Syst Man Cybern Part A Syst Hum 1999; 29(6):566–72.
[47] Gonthier Y, McPhee J, Lange C, Piedboeuf J-C. A regularized contact model with asymmetric damping and dwell-time dependent friction. Multibody Sys Dyn 2004; 11:209–33.
[48] Papetti S, Avanzini F, Rocchesso D. Numerical methods for a nonlinear impact model: a comparative study with closed-form corrections. IEEE Trans Audio Speech Lang 2011;19:2146–58.